



Modeling Cassini UVIS Interplanetary Hydrogen Ly α Observations from 1999 to 2017

Wayne R. Pryor^{1,2} , G. Randall Gladstone^{3,4} , Kurt D. Retherford^{3,4} , W. Kent Tobiska¹, Gregory M. Holsclaw⁵, and Larry W. Esposito⁵

¹ Space Environment Technologies, LLC 528 Palisades Dr., Ste 164 Pacific Palisades, CA 90272-2844, USA

² Science and Engineering Division Central Arizona College, 8470 N Overfield Road Coolidge, AZ 85128 USA

³ Southwest Research Institute, 6220 Culebra Road San Antonio, TX 78238, USA

⁴ University of Texas at San Antonio One UTSA Circle San Antonio, TX 78249, USA

⁵ Laboratory for Atmospheric and Space Physics, 1234 Innovation Drive, University of Colorado, Boulder, CO 80303, USA

Received 2023 July 23; revised 2023 November 24; accepted 2023 November 29; published 2024 January 8

Abstract

The Cassini Orbiter Ultraviolet Imaging Spectrograph (UVIS) obtained interplanetary hydrogen Ly α observations from 1999 to 2017, with mid-2004 to 2017 observations obtained from Saturn orbit. During its Saturn orbital phase, the spacecraft moved from mostly downwind and sidewind in the heliosphere to upwind. We analyze the full set of observations with our existing hot hydrogen density model with a solar illumination model most recently used to study Solar and Heliospheric Observatory Solar Wind Anisotropy Experiment data and selected Cassini UVIS observations from 2003 to 2004. We find general agreement between data and model, but with evidence for a decline in UVIS Ly α sensitivity, with a significant decline in 2002 June during a starburn event and an overall roughly linear decline in sensitivity. While earlier work by Pryor et al. fit the UVIS Ly α data from 2003 to 2004 with a hydrogen density in the outer heliosphere (but after filtration at outer heliospheric boundaries) of 0.085 cm^{-3} using the UVIS laboratory sensitivity calibration, including the sensitivity decline found here leads to a revised hydrogen density estimate of $n_{\text{H}} = 0.14 \pm 0.03 \text{ cm}^{-3}$. This density estimate is consistent with a recent neutral hydrogen density estimate near the termination shock of $0.127 \pm 0.015 \text{ cm}^{-3}$ based on models of observations of pick-up hydrogen ions from the New Horizons spacecraft.

Unified Astronomy Thesaurus concepts: [Heliosphere \(711\)](#)

1. Introduction

Interplanetary hydrogen Ly α is a bright ultraviolet (UV) emission at 121.6 nm, with a distinctive spatial emission pattern due to the flow of interstellar wind hydrogen through the solar system that has been modeled by several research groups, as reviewed in Izmodenov et al. (2013), Quémerais et al. (2013), and Baliukin et al. (2022). The contribution of galactic Ly α has generally been assumed to be a minor component in the signals seen in the solar system (e.g., Thomas & Blamont 1976; Lallement et al. 2011). However, Gladstone et al. (2013, 2018, 2021) reported that the New Horizons, Voyager 1, and Voyager 2 spacecraft exploring the outer heliosphere (Figure 1) see only a very gradual falloff with upwind radial distance from the Sun in Ly α , suggesting a significant ~ 43 Rayleigh (R) galactic component based on the New Horizons calibration. Figure 5 in Gladstone et al. (2021) suggests that the galactic contribution is isotropic within $\sim 25\%$. Figure 1 from Elliott et al. (2016) shows the upwind escape trajectories of New Horizons, Pioneer 11, and both Voyagers, and the Pioneer 10 downwind escape trajectory. Here (Figure 2) we have added Pioneer 10 UV Photometer (UVP) data (Gangopadhyay & Judge 1996) obtained downwind to a figure adapted from Gladstone et al. (2018), reinforcing the idea of a very gradual falloff in Ly α with distance to a substantial asymptotic value due to galactic Ly α emission.

The Cassini spacecraft also spent years in the outer heliosphere relatively close to the Sun, (Figures 1, 3, and 4), at an almost constant distance from the Sun after Saturn Orbital Insertion (SOI) in mid-2004. Pryor et al. (2008, 2022) examined 27 day solar modulations in Cassini Ultraviolet Imaging Spectrograph (UVIS) data from 2003 to 2004, with the second paper concluding that these data supported the idea of a substantial galactic background. In Pryor et al. (2022), the UVIS laboratory calibration was applied to find an initial interplanetary hydrogen estimate of $n = 0.085 \text{ cm}^{-3}$ in the model fits. In-flight stellar calibrations showed that the UVIS Far Ultraviolet Channel (FUV) laboratory calibration does not apply to the whole mission (Steffl 2005; Holsclaw 2014). In particular, the red sensitivity of the instrument improved with time, and certain parts of the detector suffered a loss in sensitivity in a starburn event when the instrument spent too long looking in the direction of the UV-bright star Spica. This paper analyzes the large set of UVIS interplanetary Ly α data obtained over the mission, compared to our standard model validated on a variety of missions, to assess the UVIS degradation at Ly α and improve our interplanetary hydrogen density estimate after correcting for degradation. This Ly α degradation curve may also prove useful in future studies of Saturn's dayglow, auroras, rings, and moons.

2. Data Sets

The Cassini UVIS FUV channel (111.5–191.2 nm) frequently obtained interplanetary hydrogen Ly α data during its long cruise to Saturn after its launch on 1997 October 15 and initial instrument check-out starting 1999 January 7 and during its orbital mission at Saturn that began 2004 July 1 and ended 2017 September 15. The narrow Ly α line was spectrally



Original content from this work may be used under the terms of the [Creative Commons Attribution 4.0 licence](#). Any further distribution of this work must maintain attribution to the author(s) and the title of the work, journal citation and DOI.

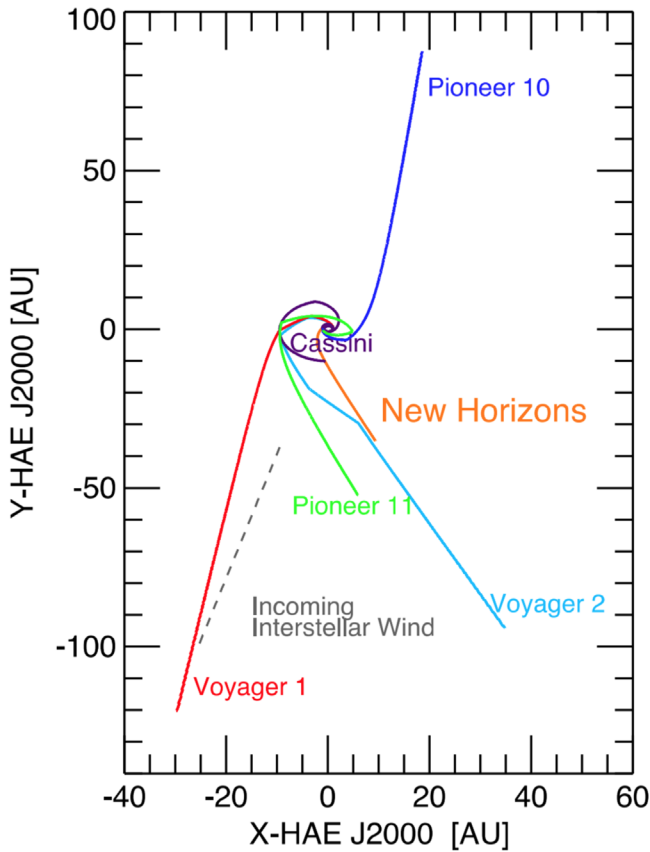


Figure 1. Trajectories of Cassini, New Horizons, and previous outer heliospheric missions (from Elliott et al. 2016). Here HAE stands for Heliospheric Aries Ecliptic coordinates. In this system the Z-axis is normal to and northward from the ecliptic plane; the X-axis extends toward the first point of Aries (the Vernal Equinox, i.e., to the Sun from Earth in the first day of Spring). The Y-axis completes the right-handed coordinate system.

unresolved, with a three-position slit mechanism providing 0.275, 0.48, and 2.49 nm spectral resolution for extended sources like interplanetary hydrogen Ly α . Data presented here were obtained with all three slits, with the FUV detector’s 1024 spectral \times 64 channels of spatial information returned in a wide variety of formats depending on available data rate. Most were obtained with the long-slit spatial information binned into a single spatial channel, containing a single partially binned spectrum. Pryor et al. (2022) examined selected cruise phase data from 2003 to 2004, when the spacecraft was generally downwind of the Sun, moving sidewind, and nearing Saturn (Figure 3). Some early orbital phase data from 2004 after SOI was included in that paper. The current paper extends the analysis to include suitable interplanetary hydrogen Ly α data from the entire mission, including both the cruise phase and the orbital phase at Saturn. Figures 3 and 4 show that while the cruise phase obtained data at a range of distances and ecliptic longitudes, the Saturn orbital phase was at a nearly constant distance from the Sun, and began downwind and somewhat sidewind of the Sun and ended upwind of the Sun.

To calibrate the data, the Cassini UVIS Ly α lab calibration was used (Esposito et al. 2004; Holsclaw 2014). Background was removed by subtracting the count rate in the last few spectral channels near 190 nm and scaling to the whole spectrum. The remaining counts per second were divided by the UVIS Ly α laboratory calibration in counts/s/R appropriate

for that slit configuration to obtain the brightness in Rayleighs (R).

3. Model

We used the same standard hot model for heliospheric Ly α described in Pryor et al. (2022). Briefly, our Ly α model (Thomas 1978; Ajello et al. 1987; Pryor et al. 1992, 2001, 2013, 2020, 2022) describes interstellar wind hydrogen passing through the solar system and illuminated by solar Ly α photons. We assumed an inflow of interstellar wind neutral hydrogen from the upwind direction 254°7 ecliptic longitude and 5°2 ecliptic latitude (in B1950 coordinates) based on measurements of the well-defined helium focusing cone by the Ulysses GAS instrument (Witte 2004). We have neglected the slight offset in the hydrogen flow direction from the helium flow direction found in Solar and Heliospheric Observatory (SOHO) Solar Wind Anisotropy Experiment (SWAN) data (Lallement et al. 2005, Lallement et al. 2010). We assumed thermodynamic parameters upwind “at infinity” in the hot model code, which neglects outer heliospheric effects. This outer boundary condition can be considered to be taken near the upwind termination shock at 90 au (inside the outer heliospheric boundaries) with values of density $n_H = 0.085 \text{ cm}^{-3}$, velocity $v = 20 \text{ km s}^{-1}$, and temperature $T = 10,000 \text{ K}$ (for discussions of v and T see, e.g., Clarke et al. 1998; Costa et al. 1999). We note that $T = 10,000 \text{ K}$ for hydrogen is larger than the standard value of $T = 7500 \text{ K}$ (McComas et al. 2015) used for interstellar wind helium due to outer heliospheric heating effects preferentially affecting hydrogen and creating a somewhat non-Maxwellian distribution (e.g., Izmodenov et al. 2013).

The time-dependent Ly α line-integrated flux is taken from the Laboratory for Atmospheric and Space Physics (LASP) solar database (Woods et al. 2000), with a correction to the estimated line-center flux (Emerich et al. 2005; Lemaire et al. 2015; Kretschmar et al. 2018). The solar line-center Ly α flux was also used to calculate the time-dependent ecliptic radiation pressure acting on the hydrogen atoms, opposing solar gravity. The ratio of the radiation pressure force to the solar gravity force is referred to as the μ parameter, with values greater than one corresponding to a net repulsive force on hydrogen atoms, and values less than one to a net attractive force. In the ecliptic plane, the computed radiation pressure values range from about $\mu = 0.8$ at solar minimum in 2010 to $\mu = 1.3$ at solar maximum in 2015. Because active regions bright in Ly α are usually found at low heliographic latitudes, it is expected that the Ly α flux over the solar poles will be lower than at lower latitudes, especially at solar maximum (Cook et al. 1981; Pryor et al. 1992). This in turn means that the radiation pressure on hydrogen atoms passing over the poles will be reduced. A time-dependent calculated estimate of the polar radiation pressure can be found by integrating over He 1083 nm equivalent-width maps (Pryor et al. 1996, 1998). For the Cassini observation period, those well-calibrated maps are not available. Pryor et al. (1996) specifically found a time-averaged polar value of $\mu = 0.75$ based on the Solar Mesosphere Explorer (SME) derived solar Ly α fluxes. Since the better-calibrated Upper Atmosphere Research Satellite (UARS) Ly α fluxes typically run $\sim 30\%$ higher than the SME-derived fluxes (Tobiska et al. 1997; Pryor et al. 1998), a better estimate for the time-averaged polar radiation pressure might be closer to $\sim \mu = 1.0$. However, estimates for the ratio of Ly α line-center

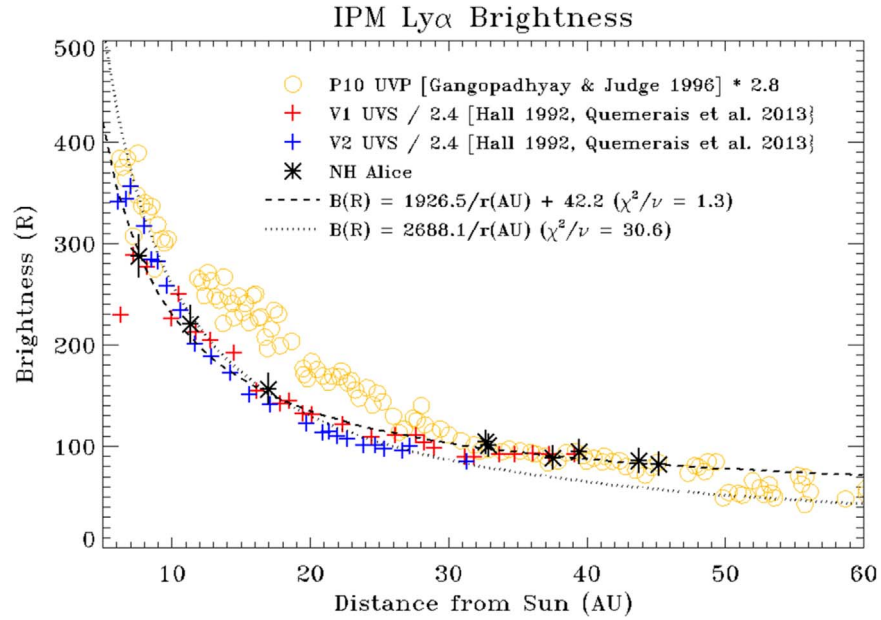


Figure 2. Brightness of interplanetary Ly α as a function of distance from the Sun in astronomical units (au) using Voyager 1 and 2, New Horizons, and Pioneer 10 data. Adapted from Gladstone et al. (2018) to include Pioneer 10 UVP data from Gangopadhyay & Judge (1996).

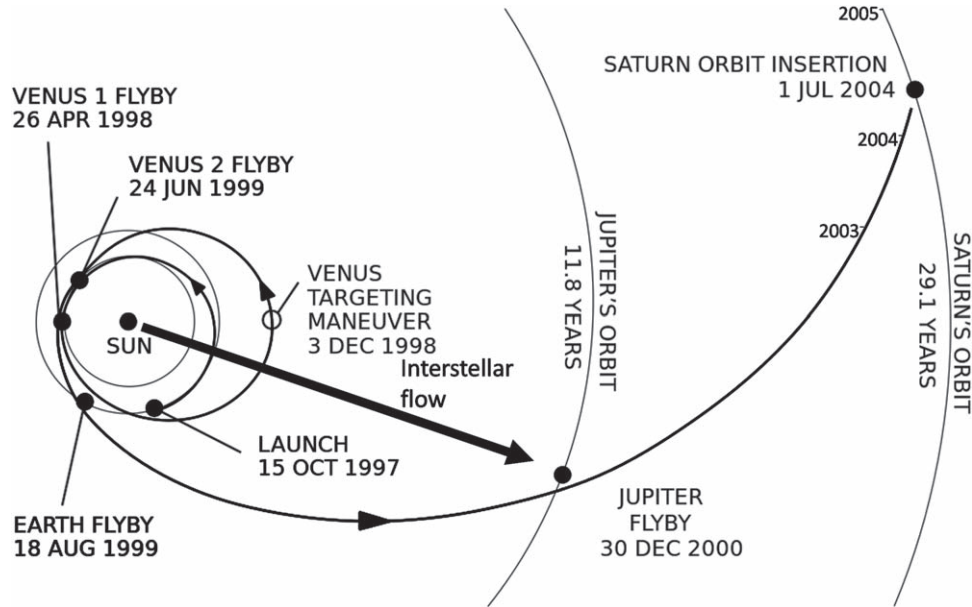


Figure 3. The Cassini spacecraft's trajectory to Saturn placed it downwind of the Sun with respect to the interstellar hydrogen flow in late 2000 during the Jupiter flyby. The view is looking from the ecliptic north down onto the ecliptic plane. The interstellar wind flow direction is indicated by the black arrow. The Cassini spacecraft was downwind of the Sun and moving sidewind in 2003–2004. Source: adapted from Wikimedia Commons to include the flow axis and the approximate Cassini locations at the start of the years 2003, 2004, and 2005.

to line-integrated fluxes have also evolved since that time (Emerich et al. 2005; Lemaire et al. 2015; Kretzschmar et al. 2018), but note that these are based on in-ecliptic observations from SOHO. We used a constant polar $\mu = 0.75$ value in the current work since it is close to but slightly lower than the in-ecliptic estimate at solar minimum of $\mu = 0.8$ and lower than the estimate at solar maximum of $\mu = 1.3$. The time-independent polar and time-dependent in-ecliptic estimates were then averaged in the model. The radiation pressure was then averaged over periods of 1–8 yr. The averaging period used was 1 yr near the Sun, with longer periods used for volume elements downstream of the Sun where the hydrogen

atoms had been exposed to a varying radiation pressure for a longer period of time. The calculation neglects the dependence of the solar radiation pressure force on the radial velocity of the H atom, as discussed in Thomas (1978), and the expected decline in radiation pressure with increasing Ly α optical depth discussed in Hall (1992).

The major loss process for slow hydrogen near the Sun is charge exchange with solar wind protons. Solar wind proton density and velocity data is taken from the National Space Science Data Center database (NSSDC; King & Papitashvili 2005). The solar-wind charge-exchange lifetime latitudinal variation is estimated using a solar wind asymmetry factor

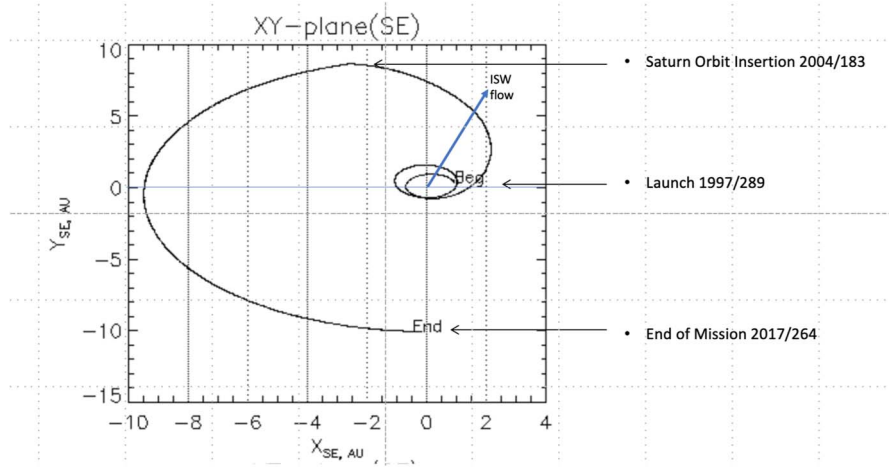


Figure 4. Here the Cassini trajectory from the entire mission is shown in solar ecliptic (SE) coordinates. The spacecraft was downwind and somewhat sideward in 2004, when Saturn orbital insertion occurred, and was roughly upwind in 2017 when the mission ended. Source: adapted from a plot generated at <https://omniweb.gsfc.nasa.gov/coho/helios/heli.html> using Cassini mission dates and solar ecliptic coordinates and then edited to include the interstellar wind (ISW) flow direction and annotated to show key mission events.

$A = 0.4$. The A parameter is defined by the expression that the hydrogen lifetime t against charge exchange with solar wind protons at a given heliographic latitude is

$$t(\text{latitude}) = t(\text{latitude} = 0) / (1 - A \sin^2(\text{latitude})),$$

which leads to a larger lifetime away from the ecliptic plane for positive values of A (e.g., Witt et al. 1979). A secondary loss process for hydrogen atoms is time-dependent EUV photo-ionization, which is estimated using the Space Environment Technologies (SET) Solar Irradiance Program (SIP; Tobiska et al. 2000; Tobiska & Bouwer 2006). The ionization rates and radiation pressure were averaged over periods of 1 yr or longer, as discussed in Pryor et al. (2013). The radiative transfer model used is fundamentally a single scattering model. However, a correction is made for multiple scattering enhancement of signal in the relatively dim downwind direction based on the angle θ between a ray from the Sun along the upwind axis to a ray from the Sun to any space point. The multiple scattering correction is discussed in Keller & Thomas (1979), Keller et al. (1981), Ajello et al. (1993), Quémerais & Bertaux (1993), Ajello et al. (1994), and calculated using multiple scattering codes (Hall 1992; Hall et al. 1993). Keller et al. (1981) demonstrated that the multiple scattering correction factor depends primarily on θ and depends very little on spacecraft position within 40 au of the Sun. Table 1 of Pryor et al. (1998) details the dependence of the correction on solar radiation pressure, hydrogen atom lifetime, and density. Those calculations assumed a hydrogen density at infinity of $n = 0.17 \text{ cm}^{-3}$, a velocity at infinity of 20 km s^{-1} , and a hydrogen temperature at infinity of 8000 K. Since that time, we have also evaluated corrections for higher temperatures of 12,000 and 16,000 K and linearly interpolated the corrections in the current work. The model run shown in this paper used a hydrogen density of $n = 0.12 \text{ cm}^{-3}$, a velocity at infinity of 20 km s^{-1} , and a hydrogen temperature at infinity of 10,000 K. Raising the temperature slightly lowers the downwind corrections. Discussions of the multiple scattering correction in Table 1 of Quémerais & Bertaux (1993) and in Pryor et al. (1998) indicate

that the corrections are only very weakly dependent on the density within 20 au of the Sun in the hydrogen density range at infinity of $0.1\text{--}0.2 \text{ cm}^{-3}$. That is, we find that linear scaling will apply in small adjustments to the derived calibration and derived density for the Cassini observations.

4. Discussion

The results of our modeling of the UVIS data are presented in Figure 5, which shows the UVIS Ly α brightnesses from 2000 to 2017 in red. Plotted points are averages of 20 observations to reduce scatter. Points were chosen to avoid points obtained within 20 Saturn radii of Saturn, to avoid look directions passing within 30 radii of a planet or the Moon, and to avoid look directions within 80° of the Sun. Some unusually low points, representing partially returned spectra, and unusually high points, representing noise hits, have also been removed. Points were also filtered to remove spectra that showed long-wavelength light attributed to stars. The corresponding model values are shown in black, where here a 43 R constant galactic background, discussed in Gladstone et al. (2018, 2021) and Pryor et al. (2022), has been added to the standard model results obtained for a density value of $n_H = 0.085 \text{ cm}^{-3}$. On this low-resolution plot, the dominant feature seen in both data and model is the slow solar cycle variation in the brightness, as the illuminating solar Ly α brightness, radiation pressure, and ionization rates vary. The overall pattern seen in this figure is general agreement in the brightness variations. The lower panel examines the ratio of the data to the model. Although there is still considerable scatter in the data, early points from mid-1999 cluster near a data/theory ratio of 1.7. The data/theory ratio crosses 1.0 in 2003–2004, in agreement with our density selection of $n_H = 0.085 \text{ cm}^{-3}$ for the 27 day variation studies and roll variation studies in that time period reported in Pryor et al. (2022). If we interpret these trend results as indicating a large decline in instrument sensitivity from launch to 2003–2004, then we should scale the derived hydrogen density in Pryor et al. (2022) obtained using the laboratory calibration upwards to $n_H = 0.085 \times 1.7 \sim 0.14 \text{ cm}^{-3}$. After 2003–2004 the ratio continues a roughly steady decline, ending the mission in 2017 near 0.6.

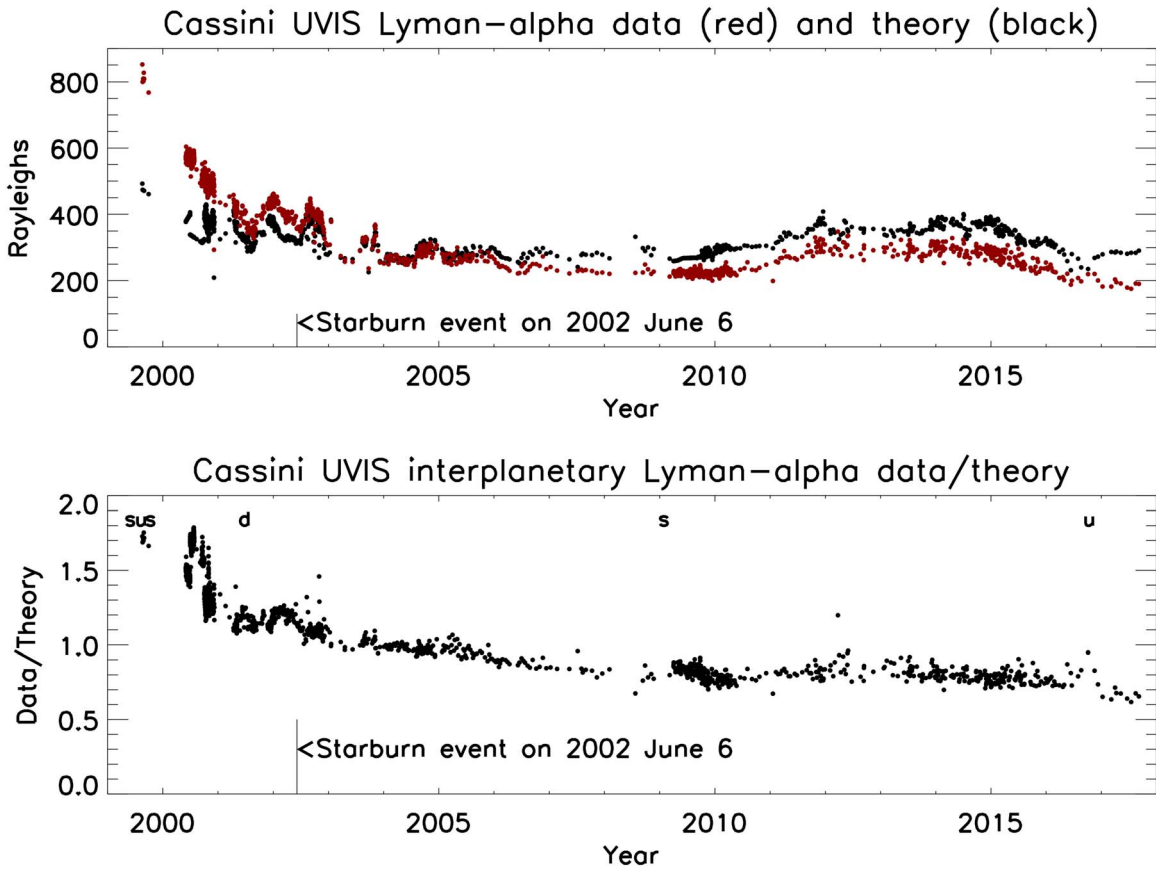


Figure 5. Top panel: Cassini UVIS interplanetary hydrogen data (shown in red) from the whole mission, compared to the standard model (shown in black) with 43 R of galactic background added. In this case, the neutral hydrogen density used is 0.085 cm^{-3} . Bottom panel: here the data has been divided by the model, showing an overall declining trend. The time of the Spica starburn event is indicated. Also shown are the labels s, u, and d, which indicate when Cassini was sideward, upwind, and downwind in the heliosphere. A typical point shown represents $\sim 20,000$ detector counts, so statistical errors are less than 1%.

We also examined the dependence of this trend on spacecraft location and look direction. Figure 5 indicates when the Cassini spacecraft was upwind, downwind, and sideways, showing that most of the data were obtained in a single slow spacecraft traverse from heliospheric downwind (2001 May 19) to upwind (2016 September 4). Figure 6 shows the ratio of data divided by theory as a function of time and look direction. The filtered look directions shown include spacecraft rolls, roughly viewing at right angles to the line from the spacecraft to the Earth and forming great circles passing near both ecliptic poles, and individual discrete spacecraft pointings in a variety of directions. The most obvious trend in Figure 6 is the declining ratio of data divided by theory, which we attribute to declining UVIS sensitivity.

An alternative interpretation of our results would be a large systematic problem in the upwind-downwind behavior of our model in addition to the loss of sensitivity from the obvious starburn event in 2002. We consider this less plausible because the model has been well-validated on a number of missions. For example, we previously applied this technique of using standard Ly α models to monitor instrument sensitivity to Galileo mission cruise and Jupiter orbital phase data from 1990 to 1997 (Pryor et al. 2001). The Galileo Orbiter had two UV spectrometers measuring interplanetary Ly α , the Ultraviolet Spectrometer (UVS) and the Extreme Ultraviolet Spectrometer (EUVS). In that case, the time series of UVS data varied in good agreement with our standard model, while the data from the more heavily used EUVS instrument showed an apparent

decline in sensitivity of about 40%, a smaller decline than we find for the longer duration mission of the Cassini UVIS in this paper. More recently, long-term studies of SWAN heliospheric Ly α data obtained near 1 au with our models (Pryor et al. 2013, 2020) have found the trends in the models generally in good agreement with the data from 2008 to 2019, within about 20%.

5. Conclusions

Here we have examined the large set of interplanetary hydrogen observations from the Cassini Orbiter UVIS. While our standard model, now including a 43 R galactic background, and the data both show brightness changes due to spacecraft location and solar cycle variations in solar Ly α emissions and other factors, the agreement between data and model is not perfect. If we assume the model is accurate, then the comparison of data and model shows an almost linear decline in UVIS Ly α sensitivity, with a marked drop in 2002. We note that a known “starburn” event occurred on 2002 June 6 when extended pointing of UVIS toward Spica degraded exposed parts of the UVIS FUV detector.

Pryor et al. (2022) made an initial interplanetary hydrogen density hot model estimate in the period 2003–2004 of $n_{\text{H}} \sim 0.085 \text{ cm}^{-3}$ inside any outer heliospheric boundary filtration, using the UVIS lab calibration (Esposito et al. 2004) and neglecting any UVIS sensitivity degradation. Modeling the full set of Cassini UVIS interplanetary Ly α data

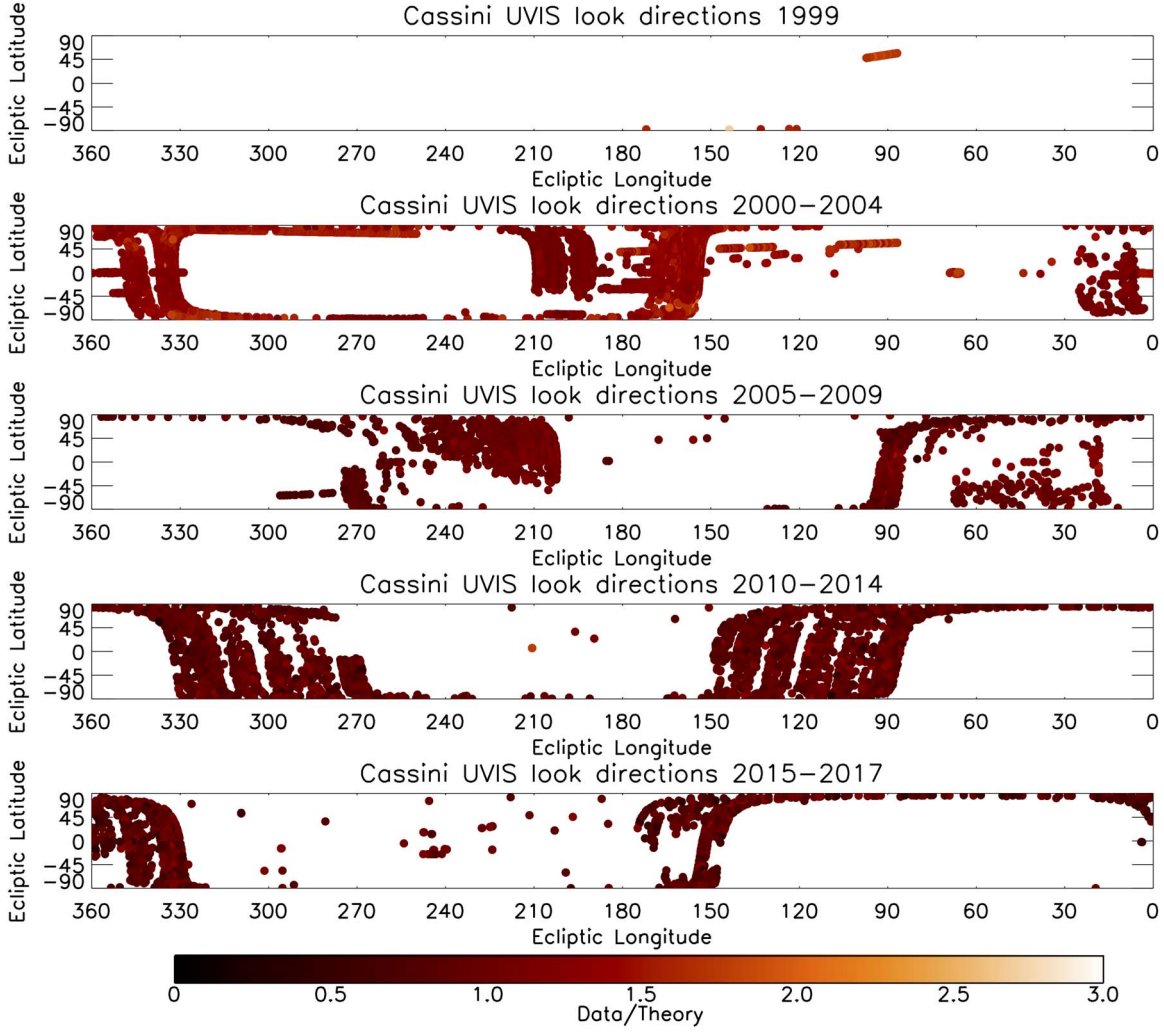


Figure 6. The filtered data shown in Figure 5 are again shown, but here distributed in the ecliptic latitude and longitude of the viewing direction. The color shown for each point indicates the ratio of data divided by theory. The panels, from top to bottom, show data points from 1999, 2000–2004, 2005–2009, 2010–2014, and 2015–2017.

from 2000 to 2017 shows the UVIS sensitivity was declining between 2000 and 2004, including a marked decline after 2002 June 6 (the starburn event, when UVIS observed Spica for too long).

This paper, including the large Cassini UVIS sensitivity loss from launch to 2003–2004, revises the interplanetary density estimate upwards to $n_H \sim 0.085 \times 1.7 \sim 0.14 \text{ cm}^{-3}$. Adding together in quadrature an assumed 12% absolute error in the Cassini UVIS laboratory calibration (McClintock 2002) and an estimated 20% error in our model trends from launch in 1999–2004 based on our ability to fit solar cycle variations in interplanetary measurements from a variety of spacecraft including Galileo (Pryor et al. 1992, 1996, 2001), Pioneer Venus (Pryor et al. 1998), and SOHO SWAN (Pryor et al. 2020) leads to an overall density error estimate of $\sim 23\%$. This leads to an overall estimate of $n_H = 0.14 \pm 0.03 \text{ cm}^{-3}$, roughly consistent with recent modeling values of $n_H = 0.12 \text{ cm}^{-3}$ used to fit SOHO SWAN Ly α data (Pryor et al. 2013, 2020). Adding in the proposed 43 R galactic background to future SWAN modeling will lead to relatively minor adjustments in the derived density, as Ly α signals measured at SOHO near Earth (e.g., Bertaux et al. 1997) are much larger than those measured by Cassini near Saturn.

Recently Swaczyna et al. (2020) analyzed the measurements of solar wind pickup protons with the New Horizons Solar Wind Around Pluto (SWAP) instrument and their modeling found a similar neutral hydrogen density at the termination shock $n_{H,TS} = 0.127 \pm 0.015 \text{ cm}^{-3}$.

The density determination made here using Cassini UVIS should be compared to earlier work. Ajello et al. (1987) and Puyoo et al. (1997) published tables of hydrogen density determinations from various spacecraft ranging from 0.023 to 0.3 cm^{-3} reflecting the large uncertainties in early UV calibration efforts and the difficulty in assessing in-flight degradation at Ly α . Those densities were in the context of hot models, such as our model (which is a variation of the Ajello et al. 1987 model), that contain a hydrogen density value “at infinity” (e.g., Thomas 1978) and neglect outer heliospheric “filtration” processes that lower the density from its interstellar value. Izmodenov & Alexashov (2015) presented three sophisticated models for filtration in the outer heliosphere in their Figure 8. Taking their preferred Model 3 that includes both the heliospheric magnetic field and heliolatitudinal variations of the solar wind leads to number densities of primary and secondary H atoms at 90 au upwind (near the termination shock) of ~ 0.035 and $\sim 0.058 \text{ cm}^{-3}$, respectively,

so the total number density at 90 au upwind is $\sim 0.093 \text{ cm}^{-3}$. Considering the density of 0.14 cm^{-3} in the LISM assumed in their model, the filtration factor is ~ 0.66 . This suggests that our Cassini UVIS hot model density determination of $n_{\text{H}} = 0.14 \pm 0.03 \text{ cm}^{-3}$ corresponds to a larger interstellar hydrogen density upstream outside the heliospheric boundaries of $\sim 0.14/0.66 = 0.21 \text{ cm}^{-3}$. There are still differing opinions on the interstellar hydrogen density; for example, models presented in Katushkina et al. (2017) used an interstellar value of 0.14 cm^{-3} , as did Model 3 of Izmodenov & Alexashov (2015), lower than the estimate of 0.21 cm^{-3} just found here.

Now that we have an estimate for the decline in Cassini UVIS sensitivity at $\text{Ly}\alpha$, it will be interesting to see how this affects studies of the Saturn $\text{Ly}\alpha$ dayglow from UVIS observations (e.g., Ben-Jaffel et al. 2023).




Acknowledgments

W.P. acknowledges past support from the NASA/JPL Cassini Project as a member of the University of Colorado–led UVIS team, and ongoing support for hydrogen $\text{Ly}\alpha$ modeling studies from the NASA LRO $\text{Ly}\alpha$ Mapping Project (LAMP) team at Southwest Research Institute (SwRI) through a subcontract to Space Environment Technologies (SET). W.P. also acknowledges ongoing support from Central Arizona College.

Data Availability

The Cassini UVIS data have been archived in NASA’s Planetary Data System (PDS). A good starting point can be found at pds-rings.seti.org/cassini/uvis/access.html.

ORCID iDs

Wayne R. Pryor  <https://orcid.org/0000-0001-8112-8783>
G. Randall Gladstone  <https://orcid.org/0000-0003-0060-072X>
Kurt D. Retherford  <https://orcid.org/0000-0002-1939-6813>

References

- Ajello, J. M., Pryor, W. R., Barth, C. A., et al. 1994, *A&A*, **289**, 283
Ajello, J. M., Pryor, W. R., Barth, C. A., Hord, C. W., & Simmons, K. E. 1993, *AdSpR*, **13**, 37
Ajello, J. M., Stewart, A. I., Thomas, G. E., & Graps, A. 1987, *ApJ*, **317**, 964
Baliukin, I., Bertaux, J.-L., Bzowski, M., et al. 2022, *SSRv*, **218**, 45
Ben-Jaffel, L., Moses, J. I., West, R. A., et al. 2023, *PSJ*, **4**, 54
Bertaux, J. L., Quémérais, E., Lallement, R., et al. 1997, *SoPh*, **175**, 737
Clarke, J. T., Lallement, R., Bertaux, J.-L., et al. 1998, *ApJ*, **499**, 482
Cook, J. W., Meier, R. R., Brueckner, G. E., & VanHoosier, M. E. 1981, *A&A*, **97**, 394
Costa, J., Lallement, R., Quémérais, E., et al. 1999, *A&A*, **349**, 660
Elliott, H. A., McComas, D. J., Valek, P., et al. 2016, *ApJS*, **223**, 19
Emerich, C., Lemaire, P., Vial, J.-C., et al. 2005, *Icar*, **178**, 429
Esposito, L. W., Barth, C. A., Colwell, J. E., et al. 2004, *SSRv*, **115**, 299
Gangopadhyay, P., & Judge, D. L. 1996, *ApJ*, **467**, 865
Gladstone, G. R., Pryor, W. R., Hall, D. T., et al. 2021, *AJ*, **162**, 241
Gladstone, G. R., Pryor, W. R., Stern, S. A., et al. 2018, *GeoRL*, **45**, 8022
Gladstone, G. R., Stern, S. A., & Pryor, W. R. 2013, in *Cross-Calibration of Far UV Spectra of Solar System Objects and the Heliosphere*, ed. E. Quémérais, M. Snow, & R. M. Bonnet (New York: Springer), 177
Hall, D. T. 1992, PhD thesis, Univ. of Arizona
Hall, D. T., Shemansky, D. E., Judge, D. L., Gangopadhyay, P., & Gruntman, M. A. 1993, *JGR*, **98**, 15185
Holsclaw, G. M. 2014, The Cassini UVIS User’s Guide, 21, https://pds-rings.seti.org/cassini/uvis/1-UVIS_Users_Guide_2018-Jan%2015-For%20PDS-REV-2018-07-06.pdf
Izmodenov, V. V., & Alexashov, D. B. 2015, *ApJS*, **220**, 32
Izmodenov, V. V., Katushkina, O. A., Quémérais, E., & Bzowski, M. 2013, in *Cross-Calibration of Far UV Spectra of Solar System Objects and the Heliosphere*, ed. E. Quémérais, M. Snow, & R. M. Bonnet (New York: Springer), 7
Katushkina, O. A., Quémérais, E., Izmodenov, V. V., Lallement, R., & Sandel, B. R. 2017, *JGRA*, **122**, 10921
Keller, H. U., Richter, K., & Thomas, G. E. 1981, *A&A*, **102**, 415
Keller, H. U., & Thomas, G. E. 1979, *A&A*, **80**, 227
King, J. H., & Papitashvili, N. E. 2005, *JGRA*, **110**, A02104
Kretzschmar, M., Snow, M., & Curdt, W. 2018, *GeoRL*, **45**, 2138
Lallement, R., Quémérais, E., Bertaux, J.-L., et al. 2005, *Sci*, **307**, 1447
Lallement, R., Quémérais, E., Koutroumpa, D., et al. 2010, in *AIP Conf. Proc.* 1216, Twelfth International Solar Wind Conf., ed. M. Maksimovic et al. (Melville, NY: AIP), 555
Lallement, R. E., Quémérais, E., Bertaux, J.-L., Sandel, B. R., & Izmodenov, V. V. 2011, *Sci*, **334**, 1665
Lemaire, P., Vial, J.-C., Curdt, W., Schühle, U., & Wilhelm, K. 2015, *A&A*, **581**, A26
McClintock, W. E. 2002, Cassini UVIS Calibration Report, Draft 2.2, <https://studylib.net/doc/12631315/calibration-report-cassini-uvis-draft-2.2>
McComas, D. J., Bzowski, M., Fuselier, S. A., et al. 2015, *ApJS*, **220**, 22
Pryor, W., Gangopadhyay, P., Sandel, B., et al. 2008, *A&A*, **491**, 21
Pryor, W., Stewart, I., Simmons, K., et al. 2001, *SSRv*, **97**, 393
Pryor, W. R., Ajello, J. M., Barth, C. A., et al. 1992, *ApJ*, **394**, 363
Pryor, W. R., Barth, C. A., Hord, C. W., et al. 1996, *GeoRL*, **23**, 1893
Pryor, W. R., Gladstone, G. R., Retherford, K. D., et al. 2022, *AJ*, **164**, 46
Pryor, W. R., Holsclaw, G. M., McClintock, W. E., et al. 2013, in *Cross-Calibration of Far UV Spectra of Solar System Objects and the Heliosphere*, ed. E. Quémérais, M. Snow, & R. M. Bonnet (New York: Springer), 163
Pryor, W. R., Lasica, S. J., Stewart, A. I. F., et al. 1998, *JGR*, **103**, 26833
Pryor, W. R., Tobiska, W. K., Retherford, K. D., et al. 2020, *LSPC*, **51**, 1665
Puyoo, O., Ben Jaffel, L., & Emerich, C. 1997, *ApJ*, **480**, 262
Quémérais, E., & Bertaux, J.-L. 1993, *A&A*, **277**, 283
Quémérais, E., Sandel, B. R., Izmodenov, V. V., & Gladstone, G. R. 2013, in *Cross-Calibration of Far UV Spectra of Solar System Objects and the Heliosphere*, ed. E. Quémérais, M. Snow, & R. M. Bonnet (New York: Springer), 142
Steffl, A. 2005, PhD thesis, Univ. of Colorado
Swaczyna, P., McComas, D. J., Zirmstein, E. J., et al. 2020, *ApJ*, **903**, 48
Thomas, G. E. 1978, *AREPS*, **6**, 173
Thomas, G. E., & Blamont, J. E. 1976, *A&A*, **51**, 283
Tobiska, W. K., & Bouwer, S. D. 2006, *AdSpR*, **37**, 347
Tobiska, W. K., Pryor, W. R., & Ajello, J. M. 1997, *GeoRL*, **24**, 1123
Tobiska, W. K., Woods, T., Eparvier, F., et al. 2000, *JASTP*, **62**, 1233
Witt, N., Ajello, J. M., & Blum, P. W. 1979, *A&A*, **73**, 272
Witte, M. 2004, *A&A*, **426**, 835
Woods, T. N., Tobiska, W. K., Rottman, G. J., & Worden, J. R. 2000, *JGR*, **105**, 27195